Journal of Molecular Catalysis A: Chemical 336 (2011) 87–93

Contents lists available at ScienceDirect

Journal of Molecular Catalysis A: Chemical

journal homepage: www.elsevier.com/locate/molcata

Byproducts and pathways of toluene destruction via plasma-catalysis

Haibao Huang[a,b,*], Daiqi Ye[a,**], Dennis Y.C. Leung[b], Fada Feng[a], Xiujuan Guan[a]

[a] College of Environmental Science and Engineering, South China University of Technology, Guangzhou 510006, China
[b] Department of Mechanical Engineering, The University of Hong Kong, Pokfulam Road, Hong Kong

ARTICLE INFO

Article history:
Received 12 October 2010
Received in revised form
16 December 2010
Accepted 4 January 2011
Available online 12 January 2011

Keywords:
Non-thermal plasma
Plasma-catalysis
Toluene destruction
Byproducts
Destruction pathway

ABSTRACT

To improve toluene removal efficiency and reduce byproducts, a TiO_2/γ-Al_2O_3/nickel foam catalyst was combined in and after the non-thermal plasma (NTP), leading to a plasma-driven catalysis (PDC) and plasma-assisted catalysis (PAC) process, respectively. The addition of catalysis could significantly enhance the toluene destruction with an increased CO_2 selectivity and carbon balance while the byproducts, such as O_3 and organic compounds, were dramatically reduced. The PAC exhibited the highest efficiency in toluene destruction due to the formation of more atomic oxygen and hydroxyl radicals from O_3 catalytic decomposition. The pathways of toluene destruction by NTP and plasma-catalysis were proposed according to the identified intermediates.

1. Introduction

Volatile organic compounds (VOCs) are common air pollutants that cause great harm to environment and human health [1,2]. Non-thermal plasma (NTP) has been extensively studied in VOCs pollution control in the past decades [3–5]. However, its application is greatly restricted by low energy efficiency and CO_2 selectivity as well as undesirable byproducts (such as ozone) [6–9]. An attempt to overcome these limitations is to combine NTP with catalysis [6,9,10]. This novel technique combines the advantages of high selectivity from catalysis and the fast ignition/response from plasma technique [6]. Reports on the plasma-catalysis mainly focus on the increase in energy efficiency and removal efficiency of pollutants. Few studies have been conducted on the identification and reduction of the byproducts, which may cause additional environmental pollution. In some cases, they could be more harmful than the original pollutant [11]. Fan et al. [9] investigated the BTX removal and byproducts formation on the basis of the combination of a plasma reactor energized by positive DC power supply and MnO_x/Al_2O_3 catalyst. However, the organic intermediates are not easy to be identified by conventional GC analysis method due to their trace amount. Therefore, it is vital to develop efficient ways to identify the byproducts and eliminate them. Moreover, the identified byproducts or intermediates during the reaction can be used for the study mechanism, which is still not well understood in the plasma-catalysis process. The unclear mechanism represents the challenges for a better comprehension and application for the plasma-catalysis process.

The present study aimed to eliminate the multiple byproducts during toluene destruction. A TiO_2/γ-Al_2O_3/nickel foam catalyst was combined in and after the non-thermal plasma (NTP), leading to a plasma-driven catalysis (PDC) and plasma-assisted catalysis (PAC) process, respectively. Toluene is a representative VOC pollutant and widely exists in both indoor environment and industrial processes. The characteristic of toluene destruction by NTP in the presence and absence of the catalysts was compared. Possible pathways of toluene degradation were proposed according to the identified intermediates. To the best of our best knowledge, this is the first work on the identification of organic byproducts and mechanism during toluene destruction in the plasma-catalysis process. The proposed mechanism is helpful for providing insight of VOCs destruction in the plasma-catalysis process.

2. Experimental

2.1. Experimental setup

The experimental setup is illustrated in Fig. 1. In the experiment, gaseous toluene was produced by air flux passing through pure toluene liquid (>99.5%) kept in a water bath (0 °C). High volt-

* Corresponding author at: The University of Hong Kong, Department of Mechanical Engineering, Pokfulam Road, Hong Kong. Tel.: +852 2219 4547; fax: +852 2858 5415.
** Corresponding author at: South China University of Technology, College of Environmental Science and Engineering, Guangzhou 510006, China. Tel.: +86 20 39380516; fax: +86 20 39380518.
E-mail addresses: seabao8@gmail.com, harbor@hku.hk (H. Huang), cedqye@scut.edu.cn (D. Ye).

1381-1169/$ – see front matter © 2011 Elsevier B.V. All rights reserved.
doi:10.1016/j.molcata.2011.01.002

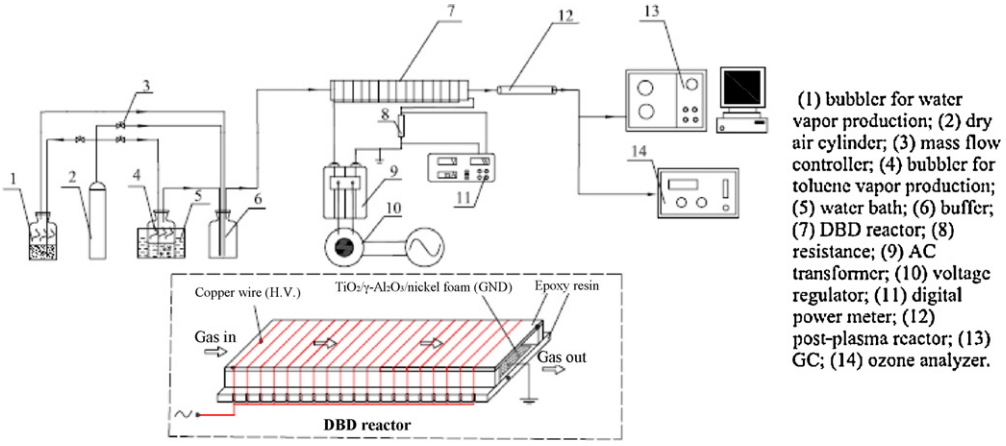

Fig. 1. Schematics of the experimental setup.

age power was supplied by a booster (0–220 V) coupled with a high voltage AC transformer (50 Hz, 30 kV) in series. A digital power meter (Everfine Photo-E-Info Co., Ltd., YF9901) was connected to the variable voltage transformer for measuring the input power. The discharge power (the power deposited to the reactor) was determined from the applied voltage and the reactor current.

A wire-plate dielectric barrier discharge (DBD) reactor was used to provide NTP in the experiment. The simplified structure of the reactor is shown in Fig. 1. The epoxy resin board, with a length of 240 mm, width of 50 mm and thickness of 0.8 mm, was used as dielectric barrier (dielectric constant $\varepsilon = 3.6$). The high voltage electrode was made of copper wire with 0.8 mm in diameter. The wire-to-wire distance was 10 mm. A piece of copper mesh (150 mm × 25 mm × 2 mm) was stuck on the epoxy resin board and acted as the grounded electrode. The gap spacing of discharge was 10 mm. The post-plasma was the area downstream from the discharge zone [12,13]. The post-plasma reactor was cylindrical and connected to the DBD reactor in series. This reactor was made of quartz glass, with an inner diameter of 28 mm and an effective length of 150 mm. A TiO_2/γ-Al_2O_3/nickel foam catalyst mesh was placed in plasma or post-plasma area (see Fig. 1) to carry out the PDC and PAC process, respectively.

The air flow rate, initial toluene concentration and humidity were 0.2 L/min, 50 ppm and 1 wt.%, respectively. Experiments were carried out at room temperature and atmospheric pressure. Gas samples from the outlet were analyzed on-line by a gas chromatograph (GC, Kechuang Chromatograph, GC-900A) equipped with two FID detectors. One detector was for organic compounds detection with a 50 m SE-30 capillary column (80 °C), and the other, equipped with a methanizer, was for carbon monoxide and carbon dioxide analysis using a 2 m carbon molecular sieve stainless steel column (65 °C). The O_3 concentration and NO_x concentration was monitored by an O_3 analyzer (Lida Instrument, DCS-1) and another GC (Haixin Chromatograph, GC-950) equipped with an ECD detector, respectively. Organic byproducts were qualitatively analyzed by a gas chromatography/mass spectrometry (GC–MS) system. Air samples from DBD reactor were collected by Summa Canisters at the energy density of 750 J/L. They were preconcentrated in a purge-and-trap system (Entech 7100 instrument) and subsequently analyzed by a GC–MS (5973N, Agilent) with an HP-5MS capillary column (Agilent, USA). The column temperature was 40 °C at the beginning, maintained for 4 min, then increased to 220 °C at 10 °C/min and maintained for 2 min. The MS detector was run in scan mode with the mass range 35–300 amu. The ionization method was electron impacting (EI). MS identification was conducted by using NIST databank (NIST/EPA/NIH Mass Spectral Library).

2.2. Catalysts preparation and characterization

Titanium dioxide used in this study was Degussa P25. It had an approximate composition of 75% anatase and 25% rutile forms of TiO_2, a BET surface area of 50 m^2/g and a primary particle size of 20 nm. TiO_2 were dispersedly loaded on the γ-Al_2O_3/nickel foam hybrid support by impregnation method. Briefly, the commercial nickel foam mesh (150 mm × 25 mm × 2 mm) was impregnated in the sol of $Al_2O_3 \cdot nH_2O$, then dried at 100 °C for 2 h and calcined at 550 °C for 4 h to get γ-Al_2O_3/nickel foam hybrid support. TiO_2 was put into distilled water and dispersed fully in an ultrasonic cleaner bath to get 8 wt.% TiO_2 slurry. The γ-Al_2O_3/nickel foam support was dipped into the TiO_2 slurry, impregnated for 30 min and then dried in an oven at 100 °C for 2 h. Thus, the TiO_2/γ-Al_2O_3/nickel foam catalyst is prepared and the weight of supported TiO_2 is 0.45 g.

The prepared catalysts were characterized with field emission scanning electron microscopy (SEM) (LEO, 1530 VP). Chemical composition analysis of the catalysts surface was performed with an energy disperse X-ray spectroscopy (EDX) analyzer (Oxford, Inca 300) associated to SEM.

Toluene removal efficiency (TRE), carbon balance, CO_2 selectivity and energy density were defined as follows:

$$\text{Toluene removal efficiency : TRE (\%)} = \frac{[\text{toluene}]_{\text{inlet}} - [\text{toluene}]_{\text{outlet}}}{[\text{toluene}]_{\text{inlet}}} \times 100\% \quad (1)$$

$$\text{Carbon balance : carbon balance (\%)} = \frac{[\text{CO}] + [\text{CO}_2]}{7([\text{toluene}]_{\text{inlet}} - [\text{toluene}]_{\text{outlet}}} \times 100\% \quad (2)$$

$$\text{CO_2 selectivity : S_{CO_2} (\%)} = \frac{[\text{CO}_2]}{7([\text{toluene}]_{\text{inlet}} - [\text{toluene}]_{\text{outlet}})} \times 100\% \quad (3)$$

$$\text{Energy density : ED (J/L)} = \frac{\text{discharge power (W)}}{\text{gas flowrate (L/min)}} \times 60 \quad (4)$$

3. Results and discussion

3.1. Catalysts characterization

Fig. 2a presents a SEM image of the TiO_2/γ-Al_2O_3/nickel foam catalyst. It illustrated that the catalyst had a pentagonal framework,

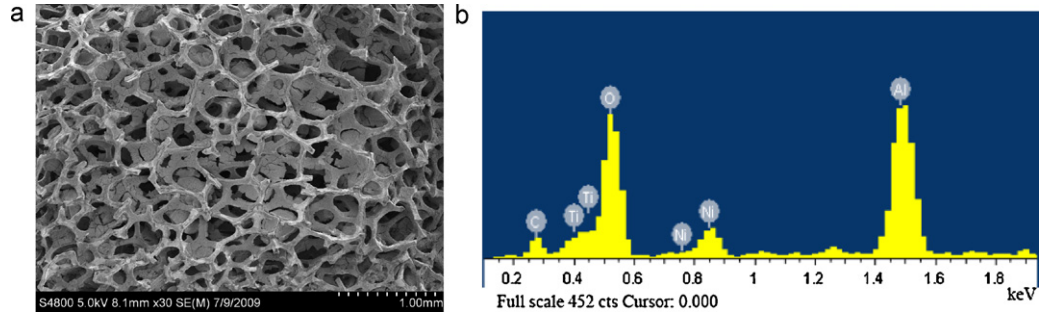

Fig. 2. (a) SEM graph and (b) EDX spectrum of γ-Al_2O_3/nickel foam supported TiO_2.

and there were a lot of small holes on the nickel foam. This catalyst owned the advantages such as low pressure drop and high surface-area-to-volume ratio. Such 3D structure can improve the molecular transport of reactants and products. The air pollutants can be adsorbed and enriched on the catalyst, resulted in increasing the destruction rate of toluene. Fig. 2b shows the EDX spectrum of γ-Al_2O_3/nickel foam supported TiO_2. The characteristic peaks in the spectrum were mainly associated with Ti, O, Ni and Al. The quantitative analysis revealed that the atomic ratio of Ti was 15.64%, indicating that the surface of catalyst was covered with TiO_2.

3.2. Enhanced destruction of toluene

3.2.1. Characteristic of toluene destruction

The toluene removal efficiency (TRE) at steady-state conditions in NTP, PDC and PAC is compared, as shown in Fig. 3a. It can be seen that the TRE increased with the increase of energy density in all cases. It is well-known that the increased energy density is helpful for the formation of more electrons with higher energy. With the increase of energy density from 61 to 1527 J/L, the TRE in NTP alone correspondingly increased from 17% to 74%.

Compared with NTP alone, the TRE was remarkably improved in the plasma-catalysis process. With the increase of energy density from 61 to 1527 J/L, the TRE increased from 20.5% to 94% in the PDC process and from 28.5% to 96% in the PAC process, respectively. The TRE obtained a maximum increase of 27% at the energy density of 412 J/L in the PDC, when compared with NTP alone. In the PDC process, there are more pathways to destruct toluene besides energetic electrons. O_3, due to its powerful oxidation ability, acts as the main oxidant instead of O_2. It can be decomposed by catalysts and generate highly active atomic oxygen. In addition, the catalyst has a strong adsorption capacity for both toluene and O_3. The adsorption by the catalyst can prolong the retention time of toluene and O_3, and improve the removal efficiency because of the higher collision probability between toluene molecules and active species [6]. Compared the PDC process, the TRE in the PAC was further increased by about 8%. In this condition, toluene destruction process can be divided into two stages: firstly, toluene was directly attacked by energetic electrons and reactive species (such as O_3) formed in the NTP; secondly, unreacted toluene was further destructed in post-plasma stage via catalytic ozonation process. In the post-plasma stage, O_3 can be catalytically decomposed into highly active atomic oxygen [11,14]. Therefore, the O_3 concentration should be consequently reduced. This claim is verified by Fig. 3b. Compared with NTP alone, the O_3 concentration in the plasma-catalysis is greatly reduced, especially in the PAC process. O_3 was decomposed by the catalyst and the resulted atomic oxygen can further be involved in the toluene destruction. This is the reason why the PAC process exhibited the highest TRE. It can be seen that the TRE is closely related to the amount of O_3 decomposition when compared with Fig. 3a and b.

It also can be found from Fig. 3a that the gap of TRE between NTP in the presence and absence of a catalyst is not significant at low energy density, in which O_3 concentration is low and toluene destruction mostly attributed to electron impact. Nevertheless, the gap becomes larger at higher energy density. This mainly owes to more toluene destruction resulted from O_3 catalytic oxidation at high energy density. Higher concentration O_3 was formed at high energy density (see Fig. 3b), leading to the formation of more reactive oxidants which are beneficial to the toluene destruction.

3.2.2. CO_2 selectivity and carbon balance

CO_2 selectivity demonstrates the degree of complete oxidation of pollutants. High CO_2 selectivity indicates that high conversion of toluene into CO_2. Fig. 4 shows the CO_2 selectivity and carbon balance in NTP and PDC process. Poor carbon balance and CO_2 selectivity was found at low energy density, especially in NTP alone, indicating incomplete toluene oxidation. It is probably caused by insufficient reactive species formed. Carbon balance and CO_2 selectivity both increased with increasing energy density in both processes. It can be explained that more electrons with higher energy and reactive species (such as O and OH•) were formed with

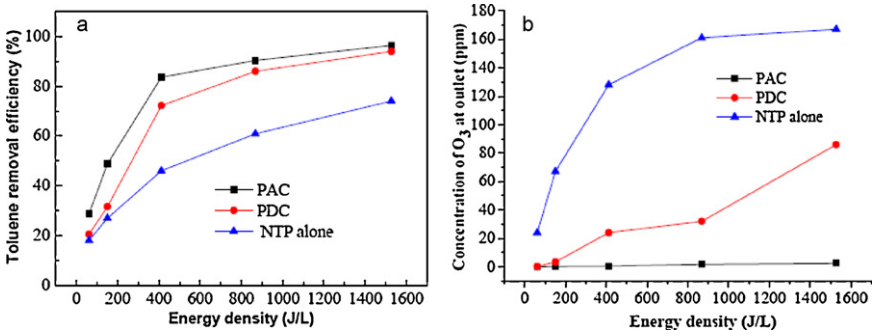

Fig. 3. (a) TRE and (b) O_3 concentration at the outlet, in the NTP, PDC and PAC process.

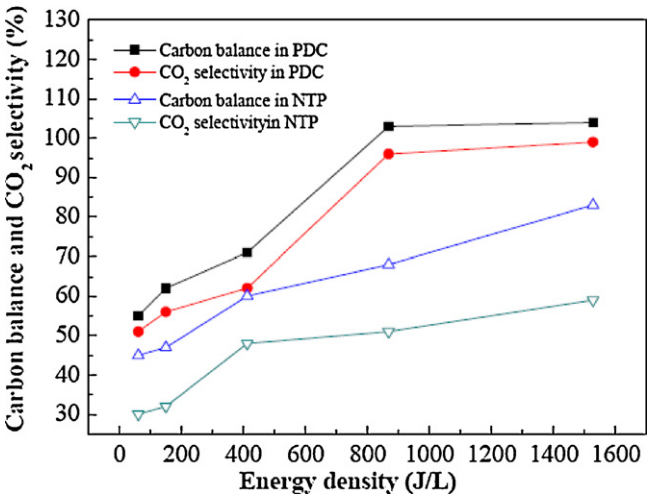

Fig. 4. Carbon balance and CO_2 selectivity in the NTP and PDC process.

increase in energy density and more toluene was oxidized into CO_2 and CO. With increase in energy density from 61 to 1527 J/L, carbon balance and CO_2 selectivity of NTP alone increased from 45% to 83% and from 30% to 59%, respectively. However, they increased from 54% to 103% and from 52% to 99%, respectively, in the PDC. Therefore, the carbon balance and CO_2 selectivity was greatly increased in the PDC in comparison with NTP alone. The improved carbon balance and CO_2 selectivity was also observed in the combined plasma catalysis system in previous study [9]. The catalysts significantly improved the mineralization of organic byproducts. Some intermediates generated from toluene oxidation were probably deposited on the catalyst surface and the reactor wall at low energy density. They were subsequently destructed by electrons with higher energy, resulting in carbon balance higher than 100% at high energy density. Similar results were also been observed in previous study [15]. Good carbon balances in the plasma-catalysis also indicated that the formation of other reaction by-products, such as aerosols and smaller organic compounds was minor.

3.3. Byproducts

3.3.1. Ozone byproduct

In the NTP process, tremendous O_3 would be formed and its concentration would be increased with increasing energy density (see Fig. 3b). With the increase of energy density from 61 to 1527 J/L, the O_3 concentration increases from 24 ppm to 167 ppm. O_3 formation in the NTP reactor proceeded via a two-step process: formation of atomic oxygen and recombination of atomic oxygen with oxygen molecule (Eqs. (5)–(7)) [16,17]:

$$O_2 + \text{electron} \rightarrow O(^1D) + O(^3P) \quad (5)$$

$$O(^1D) + M \rightarrow O(^3P) + M(M = O_2 \text{or} N_2) \quad (6)$$

$$O(^3P) + O_2 + M \rightarrow O_3 + M \quad (7)$$

where O (^{1}D) and O (^{3}P) represent excited and ground state oxygen atom, respectively.

The atomic oxygen, formed from O_2 excitation and dissociation, can also oxidize toluene. O_3 is a byproduct while it is also a strong oxidant in the system. It acts as the precursor of oxidants and plays an important role in the enhanced destruction of toluene in the plasma-catalysis process. In the PDC process, O_3 concentration is remarkably decreased due to the catalytic destruction of O_3 (see Fig. 3b). With the increase of energy density from 61 to 1527 J/L, the O_3 concentration increases from 0.3 ppm to 86 ppm. O_3 can be continuously generated while being destructed by the catalysts at the same time. Accordingly, O_3 could not be completely removed and some O_3 residue will be left behind in the effluent. However, it can be nearly eliminated at the experimental energy density in the PAC process, as shown in Fig. 3b. O_3 can be decomposed by the catalysts while there is no O_3 formation in the post-plasma. More active atomic oxygen can be formed due to O_3 destruction in the post-plasma, leading to higher TRE (see Fig. 3a).

It has been reported that O_3 can be decomposed by catalysts into molecular oxygen via atomic oxygen and peroxides (Eqs. (8)–(10)), where * denotes an active site on the catalyst surface [14]:

$$O_3 + * \rightarrow O* + O_2 \quad (8)$$

$$O* + O_3 \rightarrow O_2 + O_2* \quad (9)$$

$$O_2* \rightarrow O_2 + * \quad (10)$$

Atomic oxygen is highly active and involved in toluene oxidation. In addition, it can also react with water to form hydroxyl radical (Eq. (11)) [2]:

$$O + H_2O \rightarrow 2OH^{\bullet} \quad (11)$$

The hydroxyl radicals are very powerful oxidants that enhance toluene destruction.

Table 1
Organic byproducts of toluene destruction and their relative abundance.

Time (min)	Byproducts	Relative abundance ($\times 10^5$)	
		NTP	PDC
4.886	Acetic acid	2.2	0.25
6.007	Formic acid	7.5	2.4
6.250	Nitromethane	1.9	n.d.
7.088	2-Butanone	0.2	n.d.
7.549	2-Methylamylene	0.4	0.1
8.857	Benzene	8.7	4.4
10.453	Cetyl alcohol	0.5	n.d.
16.982	Benzaldehyde	0.3	2.9
17.160	Phenol	0.2	n.d.
17.455	Benzonitrile	0.2	n.d.
20.398	Nitrobenzene	0.1	n.d.
20.967	n-Nonaldehyde	0.9	n.d.

n.d.: not detected.

3.3.2. Organic byproducts

Fig. 5 shows the GC–MS chromatogram of the organic byproducts of toluene destruction in the NTP and PDC process. The detected species and their relative abundance were listed in Table 1. 12 types of organic byproducts from toluene destruction by NTP alone were identified by GC–MS. The abundance of benzene and formic acid is the largest in the NTP process. Among the various byproducts, benzene and nitrobenzene were primarily identified in the present work. Many by-products formed in the NTP process were also identified in previous studies [18,19]. The application of NTP is greatly limited by the presence of byproducts [6,12]. The types of gaseous organic byproducts greatly decreased in the PDC, compared with the NTP alone. It can be seen from Table 1 that only 5 types of intermediates were identified. The main byproducts included benzene, formic acid and benzaldehyde. It can be found from Table 1 that the relative abundance of benzene and formic acid were remarkably reduced in the PDC. They dropped from 870,000 to 440,000 and from 750,000 to 240,000 in the PDC, respectively, compared with that of NTP. The GC–MS results agreed well with carbon balance and CO_2 selectivity. Less organic byproducts indicated that toluene was oxidized into CO_2 and CO more completely, and carbon balance and CO_2 selectivity were accordingly raised in the PDC. In the NTP, energetic electrons were one of the main reactive species responsible for toluene destruction [20]. In case of PDC, more oxidative species such as atomic oxygen and $OH^{\bullet}$ can be generated due to the catalytic O_3 decomposition in the PDC. It should

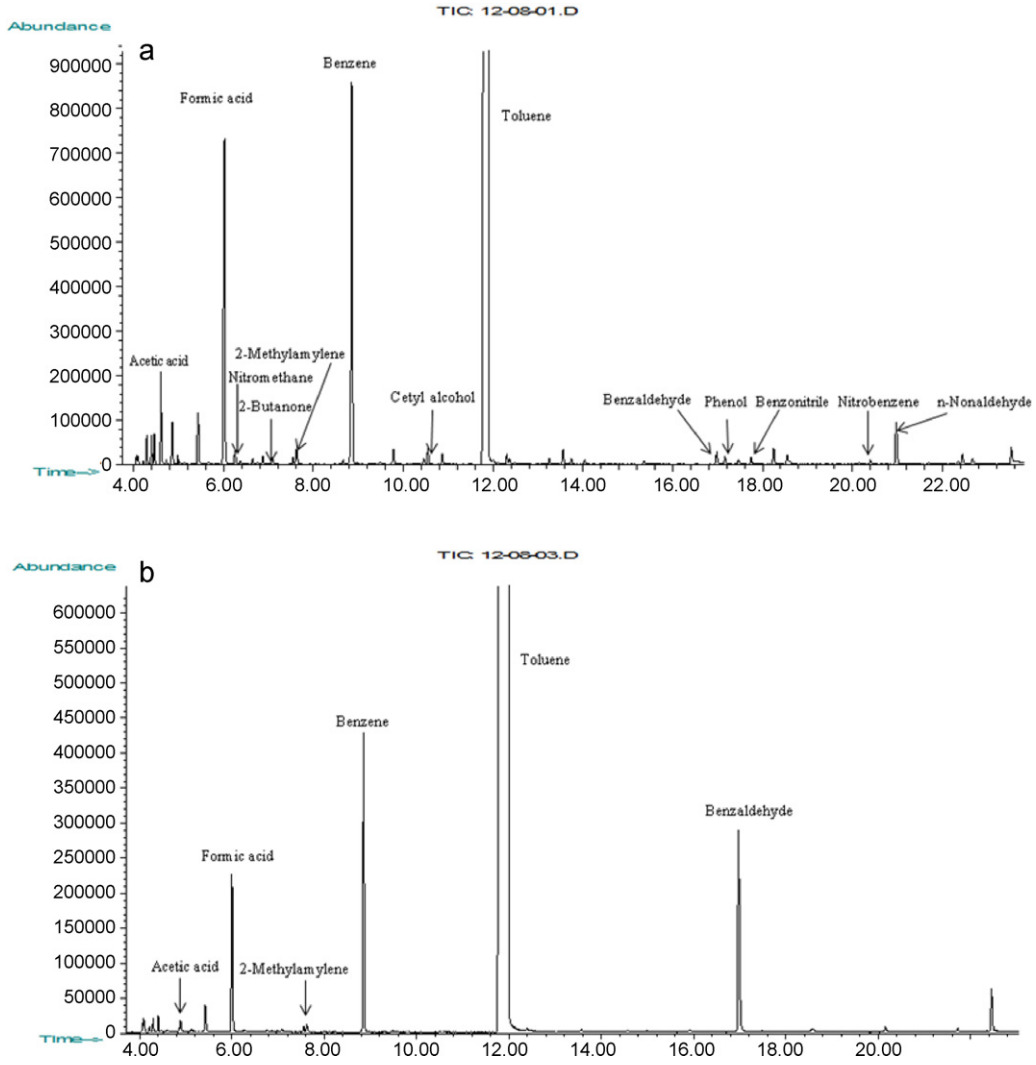

Fig. 5. GC–MS chromatogram of organic byproducts of toluene destruction in the process of: (a) NTP alone and (b) PDC.

be noted that nitrogen-containing byproducts were identified in NTP alone but not in the PDC. The combination of catalyst with NTP can generate abundant highly active oxide species and inhibit the formation of nitrogen-containing byproducts.

3.3.3. NO_x byproducts

Formation of nitrogen oxides (such as NO, NO_2, N_2O, and N_2O_5) is unavoidable during the discharge, which are also serious air pollutants [9,10]. Fan et al. monitored the NO and NO_2 and found that their concentrations were dramatically reduced in the combined plasma catalysis process in comparison with NTP alone [9]. N_2O was further monitored in this work.

As shown in Fig. 6, N_2O concentration in NTP alone greatly increased with the increase in applied voltage, ranging from 0.51 to 3.12 ppm. In case of PDC, it was decreased compared with NTP alone. N_2O is oxidized by reactive atomic oxygen. The oxidation of N_2O is described as Eqs. (12) and (13) [21]:

$$N_2O + O \rightarrow NO \quad (12)$$

$$NO + O \rightarrow NO_2 \quad (13)$$

Fast conversion of NO_2 to NO_3^{-1} by atomic oxygen over the catalysts surface can be expected [9].

3.3.4. Correlation of byproducts formation

The formation of byproducts and their concentration are closely related. The intermediates can react and affect the types and concentration of the final byproducts. In particular, O_3 had important

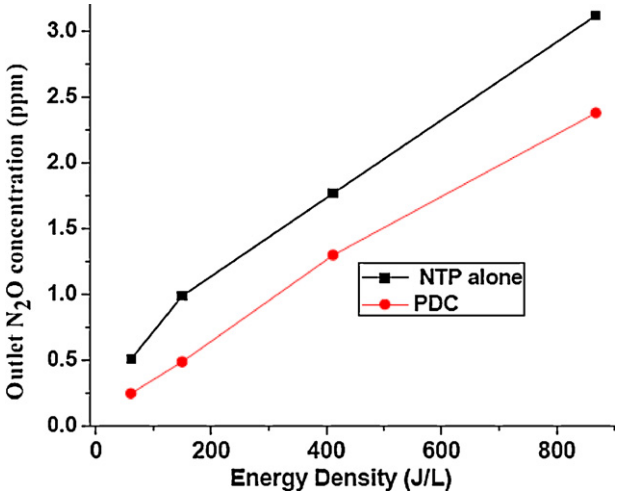

Fig. 6. N_2O concentrations at outlet with/without catalysts in plasma.

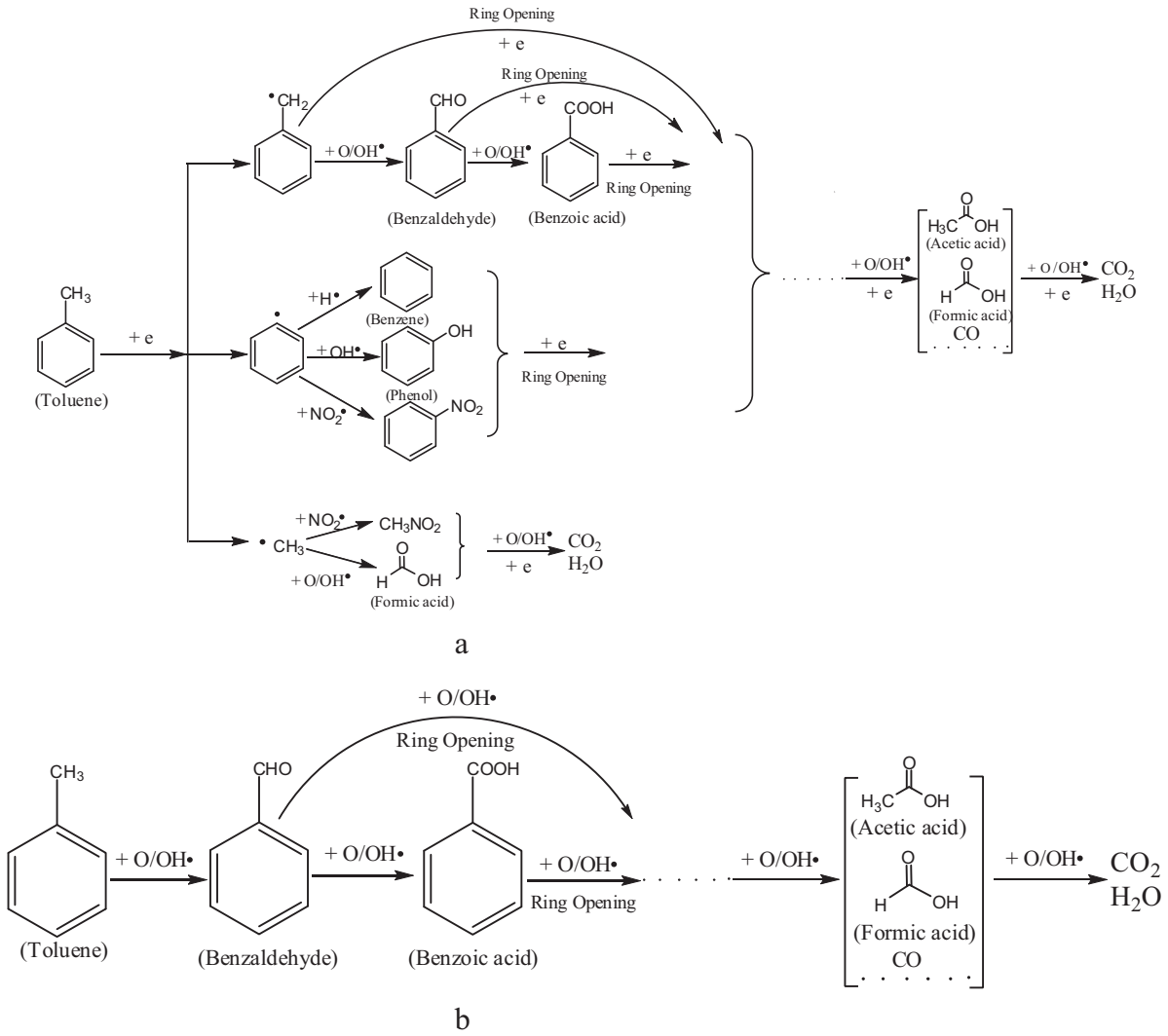

Fig. 7. Pathways of toluene destruction by: (a) energetic electrons and (b) O/OH•.

effect on the formation of other byproducts. In the NTP, the O_3 concentration increased with increasing applied voltage due to the formation of more energetic electrons. The carbon balance, N_2O and CO_2 selectivity were also improved due to the formation of more energetic electrons and reactive oxidants. Compared with NTP, the TRE, carbon balance and CO_2 selectivity were greatly improved with a decrease of byproducts in the PDC. The reduction of byproducts is closely dependent on O_3 catalytic destruction. More toluene would be oxidized into CO_2 and CO, leading to raise carbon balance and CO_2 selectivity, and less organic byproducts. The PAC process exhibits the highest efficiency in both toluene destruction and O_3 reduction. O_3 decomposition plays a vital role in both toluene destruction and byproducts elimination. In addition, nitromethane and nitrobenzene were also identified by GC–MS (see Table 1). They were probably formed from the reaction of organic compounds with nitrogen oxides.

3.4. Mechanism of toluene destruction

Different pathways of toluene destruction by NTP have been proposed according to the identified intermediates in previous studies [18,19,22]. However, they have never been proposed during plasma-catalysis process. Characteristics of toluene destruction in the PDC are greatly different from that in NTP. Apart from the destruction reactions in NTP alone, more reactions are involved in toluene destruction in the PDC. There were both homogeneous reaction in gas-phase and heterogeneous catalysis on the catalysts. Compared with NTP, more benzaldehyde was generated in the PDC. Benzaldehyde mainly formed from toluene oxidation by active atomic oxygen, but not by energetic electrons. However, the pathways of benzene formation are on the contrary. No benzene was identified in the toluene oxidation by atomic oxygen or OH• radicals [23–25].

Toluene destruction via NTP can generally be achieved through three pathways, i.e., electron-impacts, ion collisions and attacks by gas-phase radicals (such as O and OH•). The contribution of ion collisions is negligible [20]. The reaction rate constants of energetic electrons and O atom with toluene are 1×10^{-6} and 2.2×10^{-14} cm^3 mol^{-1} s^{-1}, respectively [22]. Considering the reaction rate constants together with concentration of energetic electrons and O atom, toluene has higher chances to be destructed by the former in the NTP. Therefore, electron impact should be one of the most important pathway and responsible for the initial reaction for toluene destruction [20]. O atom OH• in gas-phase are also deeply involved in toluene destruction, especially in subsequent oxidation after the opening of aromatic ring of toluene. The possible pathways of toluene destruction by the energetic electrons as dominant species are shown in Fig. 7a.

The dissociation energy of the C–H bond in methyl is 3.7 eV, which is smaller than the bond energies of C–H in aromatic ring (4.3 eV), C–C between the methyl group and the aromatic ring (4.4 eV), C–C in aromatic ring (5.0–5.3 eV) and C=C in aromatic ring (5.5 eV) [22]. The primary pathway of toluene oxidation is the H-abstraction from the methyl group by energetic electrons [26]. A hydrogen abstraction from the methyl group led to a benzyl radical which would react with O or $OH^{\bullet}$ to form benzaldehyde. Benzaldehyde can be further oxidized into benzoic acid. Those aromatic intermediates are further attacked by the energetic electrons, leading to the rupture of aromatic ring. The activated or partial decomposed species are further attacked by energetic electrons and reactive species, and are finally oxidized to CO_2 and H_2O.

Mean energy of the energetic electrons generally ranges from 1 to 10 eV [27]. C–C energy between methyl and benzene ring is 4.4 eV. Therefore, C–C can be easily destructed by energetic electrons beyond 4.4 eV, generating phenyl radical and methyl. As shown in Fig. 7a, phenyl radical could react with excited $NO_2^{\bullet}$, $H^{\bullet}$ and $OH^{\bullet}$, forming nitrobenzene, benzene and phenol, respectively, which were identified by GC–MS (Fig. 5). Excited methyl can react with $NO_2^{\bullet}$, O or $OH^{\bullet}$, forming nitromethane and formic acid, respectively, which can also be identified by GC–MS. Those aromatic intermediates will be further attacked by energetic electrons and reactive species, and finally oxidized to CO_2 and H_2O.

Much more O and $OH^{\bullet}$ radicals can be formed in the PDC, which exist both in gas-phase and on catalyst surface. Besides of energetic electrons impact, radical attack is another important mechanism leading to toluene destruction in the PDC. The possible pathways of toluene destruction by the O and/or $OH^{\bullet}$ are shown in Fig. 7b.

Benzaldehyde, formic acid and acetic acid are the main intermediates in the photocatalytic oxidation of toluene [23–25], in which $OH^{\bullet}$ is considered the main strong oxidant [28,29]. No benzene is found in the photocatalytic process. However, much benzene has been produced in NTP, as shown in Fig. 5a.

The primary pathway of toluene oxidation by $O/OH^{\bullet}$ is the H-abstraction from the methyl group, resulting in the production of benzaldehyde, which will be further attacked by an $O/OH^{\bullet}$ forming benzoic acid. The aromatic intermediates are also ruptured by $O/OH^{\bullet}$ attack, causing direct cleavage of the aromatic ring. The compounds generated after the ring opening are substances with small molecular mass, such as formic acid, acetic acid and CO. The reaction proceeds by a series of oxidation step by $O/OH^{\bullet}$ attack, finally leading to the formation of harmless CO_2 and H_2O. Benzene can be formed from toluene destruction by energetic electrons while no benzene is formed from $O/OH^{\bullet}$ attack. It is commonly known that the aromatic ring of benzene is much harder to be destructed than that of toluene [10,30]. Less refractory benzene formed in the PDC also support the argument that toluene destruction is greatly enhanced in the PDC.

Toluene destruction consists of several processes, and its destruction by energetic electrons and radicals are inseparable and cooperative due to their coexisting in the NTP and PDC.

4. Conclusions

The combination of catalysis with NTP significantly enhanced the toluene destruction with an increased CO_2 selectivity and carbon balance. The TRE, carbon balance and CO_2 selectivity obtained a maximum increase of 27%, 38% and 25% in the PDC process, respectively, when compared with NTP alone. Moreover, the catalyst dramatically reduced the byproducts such as O_3 and organic intermediates. The PAC process exhibited the highest efficiency in both toluene destruction and O_3 reduction. The enhanced effect of catalysis mainly attributed to the formation of more reactive species from O_3 catalytic decomposition. The pathways of toluene destruction in the plasma-catalysis process are different to that in the NTP alone.

Acknowledgments

The authors gratefully acknowledge the financial supports from the National Key High Technology Research and Development Program of China (grant no. 2006AA06A310), the Ph.D. Programs Foundation of Ministry of Education of China (grant no. 20070561042) and the CRCG of the University of Hong Kong (grant no. 200907176159).

References

[1] T. Guo, Z. Bai, C. Wu, T. Zhu, Appl. Catal. B: Environ. 79 (2008) 171–178.
[2] K.P. Yu, G.W.M. Lee, Appl. Catal. B: Environ. 75 (2007) 29–38.
[3] K. Urashima, J.S. Chang, IEEE Trans. Dielect. Electr. Insul. 7 (2000) 602–614.
[4] W. Mista, R. Kacprzyk, Catal. Today 137 (2008) 345–349.
[5] Y.S. Mok, C.M. Nam, M.H. Cho, I.S. Na, IEEE Trans. Plasma Sci. 30 (2002) 408–416.
[6] H.L. Chen, H.M. Lee, S.H. Chen, M.B. Chang, S.J. Yu, S.N. Li, Environ. Sci. Technol. 43 (2009) 2216–2227.
[7] T. Oda, J. Electrostat. 57 (2003) 293–311.
[8] S. Delagrange, L. Pinard, J.M. Tatibouet, Appl. Catal. B: Environ. 68 (2006) 92–98.
[9] X. Fan, T. Zhu, M. Wang, X. Li, Chemosphere 75 (2009) 1301–1306.
[10] H.H. Kim, S.M. Oh, A. Ogata, S. Futamura, Appl. Catal. B: Environ. 56 (2005) 213–220.
[11] M. Magureanu, N.B. Mandache, P. Eloy, E.M. Gaigneaux, V.I. Parvulescu, Appl. Catal. B: Environ. 61 (2005) 12–20.
[12] J. Van Durme, J. Dewulf, C. Leys, H. Van Langenhove, Appl. Catal. B: Environ. 78 (2008) 324–333.
[13] H.B. Huang, D.Q. Ye, X.J. Guan, Catal. Today 139 (2008) 43–48.
[14] S. Futamura, H. Einaga, H. Kabashima, L.Y. Hwan, Catal. Today 89 (2004) 89–95.
[15] H.H. Kim, A. Ogata, S. Futamura, J. Phys. D 38 (2005) 1292–1300.
[16] H.H. Kim, A. Ogata, S. Futamura, IEEE Trans. Plasma Sci. 34 (2006) 984–995.
[17] H.R. Snyder, S.K. Anderson, IEEE Trans. Plasma Sci. 26 (1998) 1695–1699.
[18] J. Van Durme, J. Dewulf, W. Sysmans, C. Leys, H. Van Langenhove, Chemosphere 68 (2007) 1821–1829.
[19] W. Liang, J. Li, J. Li, Y. Jin, J. Hazard. Mater. 170 (2009) 633–638.
[20] H.M. Lee, M.B. Chang, Plasma Chem. Plasma Process. 23 (2003) 541–558.
[21] K. Krawczyk, M. Mlotek, Appl. Catal. B 30 (2001) 233–245.
[22] H. Kohno, A.A. Berezin, J.S. Chang, M. Tamura, T. Yamamoto, A. Shibuya, S. Hondo, IEEE Trans. Ind. Appl. 34 (1998) 953–966.
[23] O. d'Hennezel, P. Pichat, D.F. Ollis, J. Photochem. Photobiol. A: Chem. 118 (1998) 197–204.
[24] Y. Irokawa, T. Morikawa, K. Aoki, S. Kosaka, T. Ohwaki, Y. Taga, Phys. Chem. Chem. Phys. 8 (2006) 1116–1121.
[25] J. Mo, Y. Zhang, Q. Xu, Y. Zhu, J.J. Lamson, R. Zhao, Appl. Catal. B: Environ. 89 (2009) 570–576.
[26] A. Ogata, D. Ito, K. Mizuno, S. Kushiyama, A. Gal, T. Yamamoto, Appl. Catal. A: Gen. 236 (2002) 9–15.
[27] Y.F. Guo, D.Q. Ye, K.F. Chen, J.C. He, W.L. Chen, J. Mol. Catal. A: Chem. 245 (2006) 93–100.
[28] J. Mo, Y. Zhang, Q. Xu, J.J. Lamson, R. Zhao, Atmos. Environ. 43 (2009) 2229–2246.
[29] J. Zhao, X.D. Yang, Build. Environ. 38 (2003) 645–654.
[30] A.M. Harling, V. Demidyuk, S.J. Fischer, J.C. Whitehead, Appl. Catal. B: Environ. 82 (2008) 180–189.